Limnol. Oceanogr., 53(2), 2008, 589–604

Doughnut in the desert: Late-winter production pulse in southern Lake Michigan

W. Charles Kerfoot
Lake Superior Ecosystem Research Center and Department of Biological Sciences, Michigan Technological University, Houghton, Michigan 49931

Judith W. Budd
Department of Geological Engineering and Sciences, Michigan Technological University, Houghton, Michigan 49931

Sarah A. Green
Department of Chemistry, Michigan Technological University, Houghton, Michigan 49931

James B. Cotner
Department of Ecology, Evolution, and Behavior, University of Minnesota, St. Paul, Minnesota 55108

Bopaiah A. Biddanda
Annis Water Resources Institute and Lake Michigan Center, Grand Valley State University, 740 Shoreline Drive, Muskegon, Michigan 49441

David J. Schwab and Henry A. Vanderploeg
NOAA Great Lakes Environmental Research Laboratory, 2205 Commonwealth Blvd., Ann Arbor, Michigan 48105

Abstract

Contrary to expectations of fairly uniform and unstratified waters, sea-viewing wide field-of-view sensor (SeaWiFS) and moderate-resolution imaging spectroradiometer (MODIS) imagery revealed a spatially complex chlorophyll *a* pattern, termed the "doughnut," in southern Lake Michigan during March to April. Phosphorus-rich coastal waters and sediments are entrained along gyre convergence zones and moved into deeper waters, stimulating a ring of production. Cross-lake surveys (April 2001 and April 2006) with two separate profiling instruments (vertical Seabird CTD casts, horizontal Acrobat tows) uncovered columnar patterns for Chl *a*, temperature, and other variables (colored dissolved organic matter, transmissivity) consistent with a spatially complex, rotating gyre structure. Optical plankton counter transects, plankton net tows, and sonar documented that the spatial heterogeneity extends to higher levels of food webs (zooplankton). The horizontal and vertical patterns suggest a previously unrecognized coupling between late-winter storm-induced gyre formation, coastal water plus sediment capture, and deep-water productivity. The pulse may explain how certain zooplankton species characteristic of the Great Lakes can successfully overwinter through what was previously perceived as a very unproductive and resource-stressful period. The magnitude of the winter pulse may be linked to climate change, as higher temperatures and more frequent winter storms suppress coastal ice formation and encourage movement of nutrient-enriched waters and sediments into deeper waters.

Acknowledgments

We thank Susan Hemme for the chlorophyll *a* calibration studies during the April 2006 RV *Laurentian* cruise and Aaron Hemme for sampling support. Lucille Zelazny prepared many of the figures and aided the phytoplankton identification. We also acknowledge the crews of the RV *Laurentian*, who guided us safely across Lake Michigan during a difficult time of the year.

Research was supported by NSF OCE-9726680 (NSF/NOAA EEGLE CoOP Project; National Science Foundation and National Oceanic and Atmospheric Administration Coastal Ocean Program, Episodic Events–Great Lakes Experiment) grant to W.C.K. and J.W.B.; a NOAA Coastal Ocean program grant (NOAA portion of NSF/NOAA EEGLE CoOP Project) to D.J.S.; a NSF DEB-0083731 (Biocomplexity) grant to W.C.K.; and a Michigan Seagrant Award NA16RG1145, Project R/ER-19 to W.C.K., J.W.B., and S.A.G.; and NOAA 46290000 and NSF OCE-9416614 to J.B.C. Matthew Julius (University of Michigan, School of Natural Resources) assisted on the April 2001 RV *Laurentian* cruise. GLERL contribution no. 1451.

Technological advances are allowing new insights into mesoscale physical–biotic linkages (e.g., regional groundwater seepage that maintains benthic algal mat diversity in lakes, Hagerthey and Kerfoot 1998; cholera outbreaks associated with El Niño oscillations, Pascual et al. 2000; Sahara eolian Fe fluxes that promote mid-Atlantic marine phytoplankton production, Wu et al. 2000). An active area of investigation includes remote sensing of winter phenomena in large temperate lakes during previously inaccessible months. Throughout the winter to early spring unstratified season, higher wind speeds and the absence of a thermocline allow the effects of wind action to penetrate deeper into the water column than during the summer stratified season (Beletsky and Schwab 2001; Chen et al. 2002). However, the exact nature of circulation in the Great Lakes and its relationship to late-winter production is poorly known because of hazardous research ship conditions throughout the winter season (Eadie et al. 1996; Kerfoot et al. 2004).

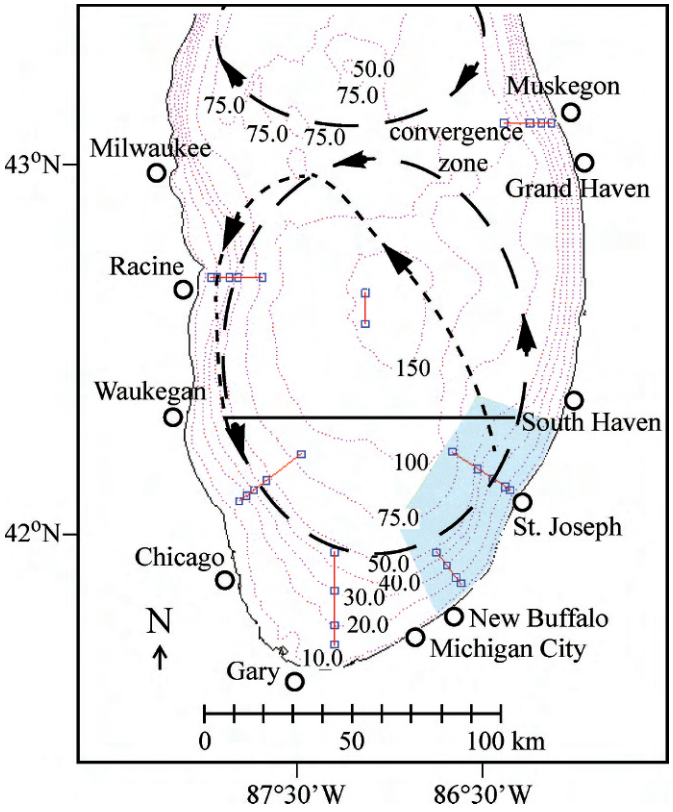

Fig. 1. Southern Lake Michigan, showing transect locations for shipboard TSM : Chl *a* validation studies (connected squares off various cities) and the April 2001, 2006 Seabird CTD/BAT transects (solid line from South Haven to Waukegan). Gyre circulation of waters after a northwest wind is indicated by arrows, with the position of the convergence zone off Grand Haven/Muskegon noted. Blue region is an intensively monitored area during the EEGLE project.

Lake Michigan has a surface area of 57,800 km^2 and a volume of 4,920 km^3, making it the third-largest North American Great Lake and the sixth-largest lake in the world. However, given the great lateral expanse of the lake relative to its average depth, we tend to forget that the aspect ratio (5812 : 1 length : depth, N-S; 2235 : 1, E-W) is really quite low. Moreover, water circulation in Lake Michigan is highly episodic because it is almost entirely wind driven. Wind direction during winter is predominantly from the north to northwest, propagating two counter-rotating gyres: a counterclockwise-rotating (cyclonic) gyre to the right of the wind in the south basin and a clockwise-rotating (anticyclonic) gyre to the left of the wind in the north basin (Fig. 1; Beletsky and Schwab 2001). After a large storm, the gyres are separated by a convergence zone along the downwind shore (Fig. 1; Grand Haven to Muskegon) with resulting offshore flow and a divergence zone along the upwind shore with onshore flow.

During the National Science Foundation (NSF)/National Oceanic and Atmospheric Administration (NOAA) Episodic Events Great Lakes Experiment, Coastal Ocean Project (EEGLE) study, sea-viewing wide field-of-view sensor (SeaWiFS) and advanced very-high-resolution radiometer (AVHRR) imagery detected a spatially complex pattern of chlorophyll (Chl *a*) and subtle temperature differences in open waters of southern Lake Michigan during late winter to early spring (Budd et al. 1999, 2002; Warrington 2001). These unexpected offshore spatial patterns were contrary to conventional notions of a well-mixed water body during winter, initially causing concern that applications of marine chlorophyll algorithms to Great Lakes freshwaters were misleading (Budd et al. 1999; Bergmann et al. 2004).

The discovery of the complicated offshore mesoscale structure coincided with detailed winter studies of persistent wind-driven coastal sediment plumes, the primary focus of EEGLE. The recurrent coastal plumes were first observed as highly reflective nearshore bands by Mortimer (1988), who believed that these structures were important to biogeochemical cycling. Subsequent investigations underscored the importance of the coastal plumes in circulating sediments (Eadie et al. 1996, 2002; Beletsky and Schwab 2001), but raised questions regarding their biological effects.

For example, the correspondence in time and space between nearshore coastal plumes and the phytoplankton spring bloom initially led to speculation that the two were connected. Mechanisms included increased availability of limiting nutrients (phosphorus) and insertion of meroplanktonic taxa via sediment resuspension (Cotner et al. 2000; Eadie et al. 2002; Millie et al. 2003). However, studies of phytoplankton photosynthesis, growth, and community structure within and outside of coastal plume waters did not find enrichment of typical spring bloom species in association with the nearshore plume (Millie et al. 2003). Moreover, modeling and field experiments suggested that reduced light availability from resuspended sediment constrained early spring phytoplankton growth rates in near-coastal environments, whereas nutrient-rich riverine inputs that were captured behind the thermal bar provided the primary stimulant for nearshore spring blooms of diatoms (Lohrenz et al. 2004).

Here we connect the nearshore plume studies with the development of an offshore "doughnut" structure, verifying a spatial association between entrainment of phosphorus-rich plumes (river water and coastal sediments) and subsequent offshore productivity pulses. Additionally, we report the results of two April (2001, 2006) cross-lake surveys that confirmed the complex spatial pattern of the so-called doughnut and revealed an underlying vertical columnar (gyre) structure. These results suggest a heretofore unrecognized large-scale coupling between gyre development, vorticity effects on resuspended sediments, chlorophyll distribution, and late-winter deepwater production. Although details will differ in other large, ice-free north temperate lakes, because of the site-specific nature of currents and resuspended sediments, the observed spatial heterogeneity prompts intriguing questions about late-winter physical–biological couplings, deep-water food webs, and implications of climate warming.

Methods

SeaWiFS/moderate-resolution imaging spectroradiometer (MODIS) imagery—Late 1980s coastal zone color scanner

Table 1. Algorithms used to calculate Chl *a* (μg L^{-1}) from remote sensing reflectance. Sensor algorithms include SeaWiFS (sea-viewing wide field-of-view sensor) and MODIS (moderate resolution imaging spectroradiometer). Reflectance (R) is indicated as the maximum of the values shown.

Sensor	Equation	R
SeaWiFS/OC2	$C_{\text{sat}} = 100^{(0.341 - 3.001R + 2.811R^2 - 2.041R^3)} - 0.04$	490/555
SeaWiFS/OC4v4	$C_{\text{sat}} = 100^{(0.366 - 3.067R + 1.930R^2 + 0.649R^3 - 1.532R^4)}$	443>490>510/555
SeaWiFS/OC2v4	$C_{\text{sat}} = 100^{(0.319 - 2.336R + 0.879R^2 - 0.135R^3)} - 0.071$	490/555
MODIS/OC3M	$C_{\text{sat}} = 100^{(0.2830 - 2.753R + 1.457R^2 - 0.669R^3 - 1.403R^4)}$	443>490/550

imagery of southern Lake Michigan uncovered a 10-km-wide plume of resuspended sediment that extended over 100 km along the southern shore (Mortimer 1988). Since becoming routinely available in 1992, AVHRR (NOAA TIROS-N series, NOAA-10 and NOAA-11) imagery has confirmed near-coastal sediment plumes and doughnut rings every year in March–April, although the spatial extent and duration has varied greatly from year to year (Eadie et al. 2002; Ji et al. 2002; Kerfoot et al. 2004). The EEGLE project focused on near-coastal sediment plume development. As part of the EEGLE project, we processed all available AVHRR (1992–2001) and SeaWiFS (1997–2000) imagery on plume development in southern Lake Michigan (Kerfoot et al. 2004; Budd et al. pers. comm.). Data from AVHRR thermal bands (3–5) were matched against lake surface temperatures from NOAA meterological buoys to provide validation of surface temperature patterns (Leshkevich et al. 1993), whereas the visible bands (1–3) provided over 12 yr of data on coastal sediment plumes.

It was during SeaWiFS processing that we became aware of a ''doughnut-shaped'' pattern of Chl *a* in offshore waters (Budd et al. 1999, 2002). The SeaWiFS sensor was located on the PorbView-2-satellite, which imaged the Great Lakes between 17:30 and 19:30 h coordinated universal time (Gregg 1992; approximately the same as Greenwich mean time). The instrument had a local area scan coverage of 2,800 km, a nadir resolution of 1.1 km^2, and was designed to improve the acquisition and accuracy of ocean color data. It is a passive, eight-band multispectral scanner that picks up reflectance (R) in six visible bands (412 nm, Gelbstoffe; 443, chlorophyll; 490, pigment; 510, chlorophyll; 555, sediments and pigments; and 670, atmospheric correction) used for estimating pigment and total suspended material (TSM) concentrations, and two near-infrared bands (765 and 865 nm) used primarily for atmospheric corrections (McClain et al. 1998).

Time series SeaWiFS imagery was processed using SeaWiFSMAP image processing software (Warrington 2001) and a modified IDL/SeaDAS (http://seadas.gsfc.nasa.gov/seadas/) code, which included the 1998 sensor calibration (McClain et al. 1998) and the coastal atmospheric correction scheme (Stumpf et al. 2000, 2003; Budd and Warrington 2004). SeaWiFS Chl *a* (C_{OC2}) maps were derived from empirical, band-ratioing algorithms, OC2v4 (O'Reilly et al. 1998, 2000*a*) and OC4v4 (O'Reilly et al. 2000*b*). The OC2v4 Chl *a* algorithm uses a ratio of SeaWiFS bands 3 and 5 (Table 1; O'Reilly et al. 1998; Budd and Warrington 2004). Concerns about coastal turbidity and dissolved organic carbon (DOC) influencing OC2 interpretations are discussed in Stumpf et al. (2000, 2003) and Budd and Warrington (2004). The spectral reflectance (R_{RS}) at 555 was used to estimate TSM (McClain et al. 1998) and was applied to help visualize the development and capture of coastal plumes after storm events.

We also examined several higher-resolution MODIS scenes over southern Lake Michigan, selecting a single one (23 April 2003) for detailed processing (Table 1; OC3 algorithms, O'Reilly et al. 2000*b*; Gumley et al. 2003) and enhancement. MODIS captures true color images at 250–500-m spatial resolution. The image presented is a monochrome version of the ''true-color'' image, which used MODIS bands 1, 3, and 4. Contrast in the visible band image was artificially stretched to enhance turbidity (TSM) patterns. Actual maximum reflectivity in the lake was on the order of 10%.

Ship-based Chl *a* and TSM samples were collected from January to November 1998–2000 along five transects off Racine, Chicago, Gary, St. Joseph, Muskegon, and at two central stations (Fig. 1). The 2006 plume transect study also featured direct Chl *a* determinations. Between 1 and 3 liters of lake water from 0–10-m depth were filtered (preweighed Whatman GFF 47 mm filters). Chl *a* was determined on a Turner model 10 fluorometer using the acid (phaeophytin) correction method (Wetzel and Likens 2000) on 90% acetone extracts and regressed against fluorometer, OC2v4, and OC4v4 values (Table 2). Calibrations were made using a pure Chl *a* standard (Sigma).

We also established a relationship between SeaWiFS C_{sat} and R_{555} estimates and in situ TSM concentrations (Table 2). This ground-truth effort provided an empirical nonlinear relationship between R_{RS} (555) and TSM ($R_{555} = 5.975\log[\text{TSM}] + 2.005$, $r^2 = 0.891$, slope average standard error [ASE] = 0.387, intercept ASE = 0.152, slope/ASE = 15.4, intercept/ASE = 13.2, $n = 32$) over the observed range of 1–12 mg L^{-1}. The logarithmic fit was heuristic in that it covered saturating values in the high-concentration coastal plume, while revealing subtle patterns for low-concentration levels in offshore waters. Additional calibrations between Chl *a* and SeaWiFS OC2, OC4v4, and MODIS OC3M used during the EEGLE project can be found in Bergmann et al. (2004). Geotiff images from the processed AVHRR and SeaWiFS imagery are posted at http://www.geo.mtu.edu/great_lakes/lakersi/cgi-bin/seawifs.cgi.

Table 2. Validation and calibration regressions for southern Lake Michigan. Coefficients of linear ($Y = bX - a$) regressions relating ship-sampled Chl *a* (μg L^{-1}) to C_{sat} (μg L^{-1}) and CTD fluorescence (FL) values. In first regression, Chl *a* measurements taken along transects at 5–10-m depth from 22 Mar 98–11 Sep 99 are regressed on C_{sat} values. In the second regression, Chl *a* measurements taken at 10-m depths along the April transect are regressed on RV *Laurentian* Seabird CTD fluorescence (FL) values. Log-linear regression relating R_{555} values to ship-sampled TSM (mg L^{-1}). TSM measurements for R_{555} validation were taken Jan–Mar 98 and Feb–Apr 99 at 5–10-m depths along coastal transects plotted in Fig. 1. All regressions are significant at the $p < 0.001$ level.

Linear regression	*n*	*b*±SE	*a*±SE	R^2
Chl *a* on C_{sat}	18	1.079±0.102	−0.087±0.171	0.874
Chl *a* on FL (CTD)	31	21.331±2.54	−0.349±0.196	0.708
Log-linear regression				
R_{555} on log(TSM)	32	5.975±0.387	2.005±0.15	0.891

Cruises examine vertical structure of the doughnut—Two cruises (April 2001, 2006) aboard the RV *Laurentian* investigated the spatial nature of the doughnut pattern along essentially the same latitudinal transect. Both cruises originated from the eastern port of Muskegon, Michigan. The cruises traversed along a mean latitude of 42.372° from South Haven to Waukegan (Fig. 1) and back, cutting across the center of the doughnut on 19–21 April 2001 and along its southern ring on 12–15 April 2006. Over the 3-d cruises, Seabird SBE 911plus conductivity-temperature-depth (CTD) full vertical profiles were taken from 64 stations at 1.85-km (1 nautical mile) intervals (longitude 87.745°W to 86.320°W). The Seabird CTD instrument package recorded depth, temperature, Chl *a* fluorescence, photosynthetically available radiation (PAR), and transmissivity. The device was equipped with a SeaTech transmissometer and Biospherical Instruments scalar PAR sensor (400 to 700 nm). Contour plots were generated from the vertical CTD casts using Matlab (Mathworks). The CTD data were binned at 0.5-m depth intervals from casts every 1.85 km for a total of 10,401 points for each parameter. Data were interpolated in the horizontal dimension using the cubic polynomial function to provide 31,975 points for contouring.

In addition to CTD vertical casts, we towed a BAT (Sea Sciences Acrobat) in tow-yo undulating fashion (5–20-m depth amplitude) behind the ship in 2001 and horizontally (10–20-m depth) in 2006, obtaining independent temperature, Chl *a*, and concentration of dissolved organic matter (CDOM) fluorescence estimates. The BAT tows traversed the same CTD transect in the reverse direction from east to west in 2001 (longitude 86.50°W to 87.75°W) at about 2.5 m s^{-1}. Contour plots were generated from the horizontal Acrobat data using the same Matlab cubic polynomial function (Matlab, Mathworks). The horizontal data were binned into 1-s time bins and gridded to 0.25 m in the vertical and 16 m in the horizontal dimension (total of 21,488 points for each variable from the Seabird CTD on the BAT). The BAT tows were important because they were independent of the vertical Seabird CTD casts and provided direct, continuous horizontal recordings. As such, they addressed concerns that processing of Seabird CTD data might create vertical artifacts. Although restricted to 5–20-m depth, the BAT tows sampled as intensively over the horizontal interval as the vertical Seabird CTD casts, providing complementary coverage. Note that in 2001, there was a slight offset in the two data sets. The eastern edge of the BAT transect corresponded to longitude 86.5°W, compared with the vertical Seabird CTD cast eastern edge of longitude 86.3°W, i.e., the CTD transect series was further east.

The BAT also contained an optical plankton counter (OPC; Mini Optical Plankton Counter, model OPC-2T, Focal Technologies) that counted and sized zooplankton, utilizing a flow-through tunnel with a thin rectangular light beam (4 × 20 mm cross-section) that measured the profile area of each plankton target, and converted the size into an equivalent spherical diameter (ESD). The device was towed at around 2.5 m s^{-1} (ca. 4–5 knots). Counts (2,119,359) were binned in two different size categories (bin 1, 0.250–0.500 mm: 1,341,627 counts; bin 2, 0.500–1.000 mm: 775,770 counts). Concentrations (counts m^{-3}) were plotted as a 50-interval mean and high–low range of 10-s-duration counts, where each 10-s count averaged 335 (bin 1) or 194 (bin 2) targets. Thus absolute and relative counts could be compared across the doughnut transect to see if there was spatial heterogeneity in larger planktonic (zooplankton) food-web components. In April 2006, vertical zooplankton tows were also taken at 24 stations along the E-W transect with a 1-m-diameter Puget Sound plankton net (125 μm Nitex). The vertical tows concentrated on contrasting assemblages in the southern doughnut ring with ones at clear water stations outside the ring. The samples were also used to determine densities and to indicate taxa in the OPC bin counts. Zooplankton net hauls (75 μm, 125 μm) in the doughnut were often clogged with large diatoms, so these were identified to genus. Likewise, phytoplankton samples were taken at 10-m depth and preserved in Lugol to quantify prominent phytoplankton associated with the offshore bloom.

Nutrient sources: Sediment resuspension and river-water experiment—A third cruise was conducted on 21 March 2000 to collect surficial sediment, offshore lake water, and river water for a microcosm experiment. The experiment tested whether admixture of river water or sediment resuspension (or both) influenced the rate of algal growth. Lake water and sediments were collected at a 45-m-deep station (NB45) located at 41.96°N, 86.81°W offshore of New Buffalo, Michigan (Fig. 1). Undisturbed surface sediments were sampled with a box corer and the top 0.5 cm was aspirated from the surface into a clean vacuum flask. Sediments were composited from three box cores to compile sufficient material. River water was taken from the St. Joseph River. All water samples were collected with 30-liter Niskin bottles and transferred to polypropylene carboys and stored dark and cold until processed at the lab approximately 6 h after collection.

The experimental design included four treatment groups consisting of control (Lake water), sediment amended

Table 3. Initial experimental conditions and river-water components for mesocosm experiments (TSM, total suspended matter; Cl, chloride concentration; TDP, total dissolved phosphorus; DOC, dissolved organic carbon). Treatments in microcosm experiments involved addition of coastal sediments and river water to lake water. See Fig. 9 for effects of experimental treatments on primary production.

		Microcosm treatments			
	Riverine source	Lake water	+Sediment	+River	+River+Sediment
TSM (mg L^{-1})	15.0	1.2	34.1	5.3	38.3
Cl^- (mg L^{-1})	37.6	11.0	11.1	15.1	15.1
TDP (μg L^{-1})	9.0	1.6	1.6	2.8	2.8
DOC (mg L^{-1})	8.24	1.60	2.44	2.95	5.12

(+Sediment), river-water amended (+River), and sediment plus river-water amended (+River+Sediment) samples (Table 3). Each treatment was produced in triplicate 12-liter carboys, which were dispensed from a common mixing tank that was constantly stirred to maximize homogeneity among replicates. The +Sediment treatment was created by adding sufficient extracted sediment to raise the TSM levels to approximately 30 mg L^{-1}, which was the maximum level observed in field observations. The +River treatment was created by adding 20% (by volume) river water to the lake water. The +River+Sediment treatment consisted of adding both extracted sediment and river water at the same proportions as for the individual treatments. Initial nutrient, sediment, and chloride concentrations of the river water and offshore lake water are given in Table 3, along with the mean initial concentrations established for the three amended treatment groups. Nutrient concentrations (total dissolved phosphorus [TDP] and DOC) in the river water were more than five times higher than the background lake water and approximately doubled substrate concentrations in river-amended (+River) treatments. TSM levels in sediment-amended (+Sediment) treatments were approximately 30 times greater than for background lake water. Microcosms were subsampled immediately upon filling (T_0) and then over a time series covering 2, 4, 7, and 12 d for the final time point. Treatment carboys were incubated at the ambient temperature of collection (4.5°C) at approximately 50% of surface light under constant mixing in a large outdoor incubator. Primary production rates (PP) were estimated from increase in particulate organic carbon (POC) over time corrected for heterotrophic bacterial production by subtracting out bacterial biomass (Johengen et al. pers. comm.).

Analytical—Samples for POC and DOC were processed through precombusted (4 h at 450°C) Whatman GF/F filters. The filtrate was collected directly in precombusted glass vials and frozen until analysis. DOC concentrations were determined by high-temperature (680°C) oxidation with a Shimadzu TOC 5000 carbon analyzer (Biddanda and Cotner 2002). Filters for POC were placed in polypropylene petri dishes and frozen until analysis. Filters were thawed and soaked in 1.0 mol L^{-1} HCl and then dried at 80°C for 24 h. POC concentrations were determined on a Carlo-Erba model 1110, CHN elemental analyzer.

Nutrient and chloride concentrations were measured using standard automatic colorimetric procedures on an Auto Analyzer II as detailed in Davis and Simmons (1979). Samples for total dissolved P were digested in an autoclave after addition of potassium persulfate (5% final concentration) and then measured as for soluble reactive phosphate (Menzil and Corwin 1965). Statistical differences were determined with paired *t*-tests (JMP, Cary, NC, ver. 5.1.2).

Results

Since becoming routinely available in 1992, AVHRR imagery has confirmed coastal sediment plumes every year in March–April, although the spatial extent and duration has varied greatly from year to year, subject to storm intensity (Warrington 2001; Eadie et al. 2002; Kerfoot et al. 2004). During image processing, we noticed a complex doughnut-shaped Chl *a* feature in the middle of the southern basin region (Budd et al. 2002). For example, Fig. 2a,b shows Chl *a* images on two days that bracketed the 2001 cruise (13 and 24 April). In the center of the southern basin, the waters were relatively clear. The central region (''hole'') was surrounded by a doughnut-like ring of elevated Chl *a* concentrations. The outer margins of the doughnut were marked by a crescent-shaped band of clear water that separated the structure from the sediment-rich nearshore plumes.

Figure 2c,d presents paired Chl *a* and TSM (R_{rs} 555) images for 26 April 2002. Again, nearshore sediment plumes (high TSM) were present around the edge of the southern shoreline. The concentric Chl *a* pattern that occurred in deeper waters closely matched offshore R_{rs} 555 bands of dilute suspended matter. The image showed separation of the doughnut on many sides, yet a connection near the convergence zone at Grand Haven to Muskegon. EEGLE shipboard sampling off several coastal ports, used to verify the SeaWiFS imagery (Fig. 1, Table 2), suggested that maximum Chl *a* concentrations in the ring ranged between 1.5 and 2.5 μg L^{-1}. EEGLE station studies of nearshore coastal plumes picked up the outer ring of the doughnut on several occasions, also recording values between 1.2 and 2.4 μg Chl *a* L^{-1} (Vanderploeg et al. 2007), although the doughnut structure was not fully recognized at the time of the nearshore sediment plume studies.

The turbid nearshore plume was initiated by major winter storms resulting from prevailing north to northwesterly winds (Schwab et al. 2000; Ji et al. 2002; Chen et al. 2004a). The alongshore currents followed bottom

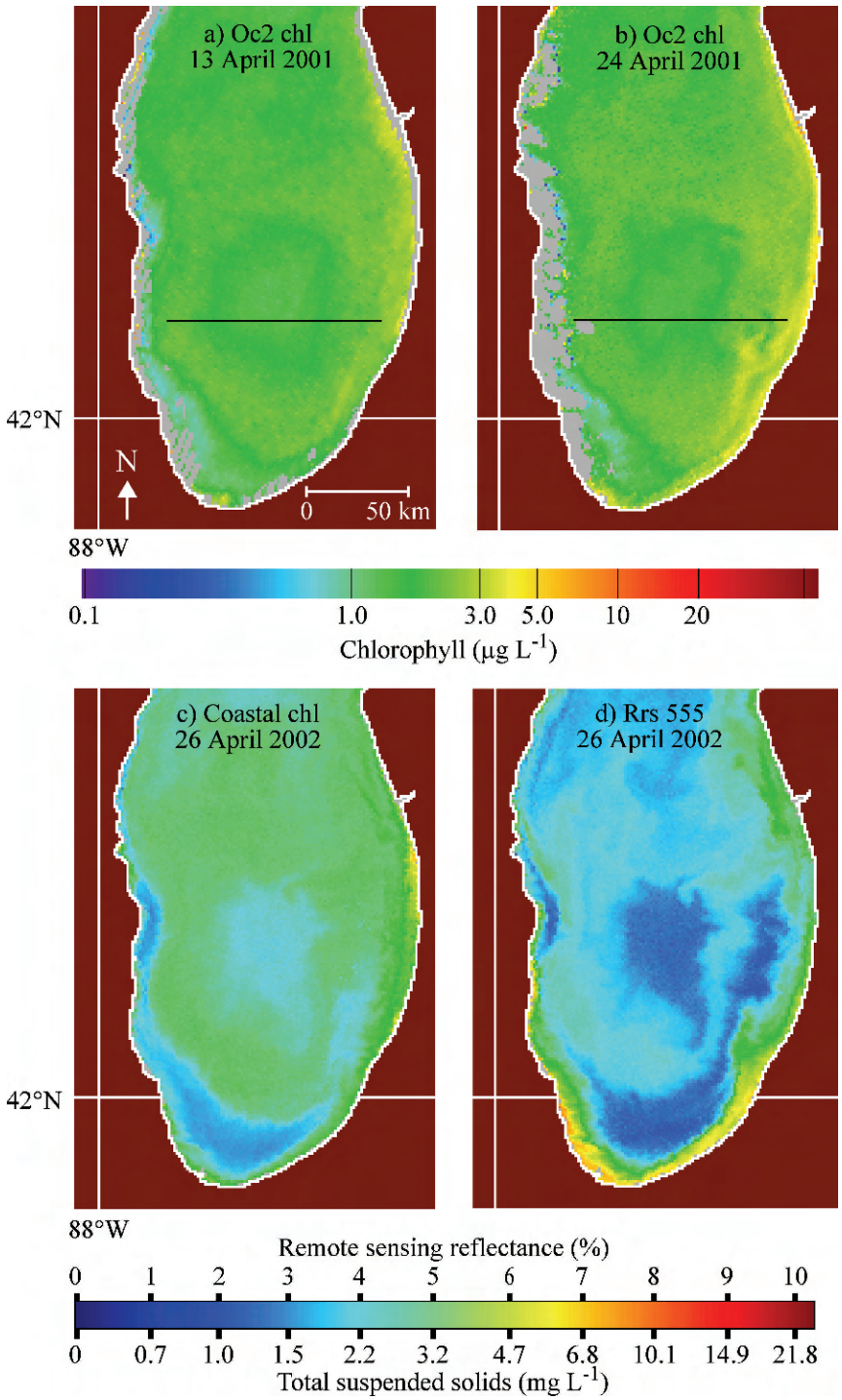

Fig. 2. Examples of doughnut-shaped ring of elevated Chl *a* concentrations from SeaWiFS imagery, as the phenomenon appears during late March–April. (a, b) The 13 and 24 April 2001 mid-lake cruise transect tracks (solid line) are superimposed upon the SeaWiFS Chl *a* images. (c, d) Panels compare Chl *a* and TSM (R_{555}) patterns on 26 April 2002.

bathymetry and could reverse direction with changes in prevailing winds (Ji et al. 2002). Coastal waters (including river discharges) were entrained and benthic nutrient-rich sediments were resuspended by storms and drawn into the counterclockwise rotation of the gyre (Beletsky and Schwab 2001; Ji et al. 2002; Kerfoot et al. 2004).

The formation of the doughnut in both images appears to be a three-step repetitive process associated with the severity of storms. The first step involves entrainment of coastal river discharges. The second step features large-scale resuspension of fine-grained bottom material in the nearshore region (depth <20 m) by wave action during

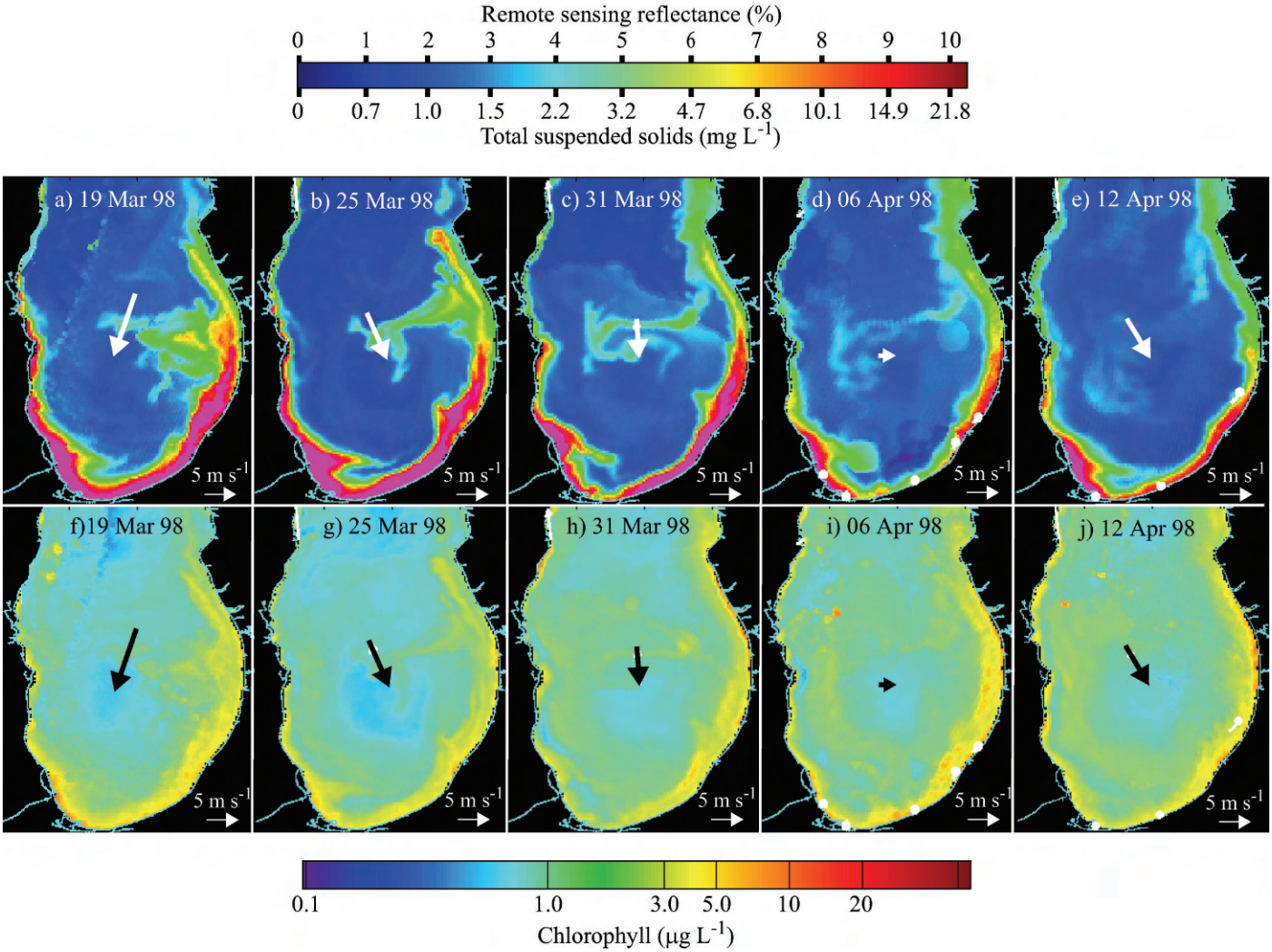

Fig. 3. (a–j) Example of offshore TSM transport and resulting Chl *a* plumes. During the El Niño episode of severe winter storms (22 March–15 April 1998), TSM is captured in the two-gyre convergence zone off Muskegon, Michigan, and drawn offshore, rotating within the southern gyre. Note the corresponding pattern for Chl *a*. Arrows show wind speed and direction.

a storm with strong winds from the north to northwest. The current circulation pattern during such a storm features southward-flowing currents in the western nearshore region with a convergence zone and offshore transport occurring somewhere along the eastern shoreline. North of the convergence zone the water seems relatively clear as it is pushed southward from the northern basin of the lake.

West and south of the convergence zone, a ring of turbid water encircles the southern basin in the nearshore zone. Nearshore concentrations of resuspended material can reach 10–30 mg L^{-1} of total suspended material. Subsequent smaller wind events that are strong enough to produce significant (5–10 cm s^{-1}) longshore currents, but not strong enough or in the wrong direction to create a large resuspension event, advect clear water from the deeper northern basin preferentially into the intermediate depth zone because currents are stronger. The third phase occurs when nearshore turbid water is captured in the convergence zone and drawn offshore, creating a ring structure. The resuspended fine-grained material can act as a visual marker, marking the paths of water movements. The turbid offshore water contains very fine-grained material (grain size <20 μm), in concentrations of 1–5 mg L^{-1}, that can stay in suspension for weeks. The turbid water forms a doughnut-shaped ring in water depths roughly between 40 and 100 m. A subsequent strong storm can create a new nearshore turbid region, or in the absence of a storm, the offshore turbidity ring can close eventually and dissipate.

An example serves to illustrate the spatial details and repetitive nature of sediment entrainment (Fig. 3). During the three-season EEGLE field study, the 08–10 March 1998 storm event was one of the largest on record, a 1-in-12-yr meteorological event (Schwab et al. 2000). Several days of intense storms produced 17 m s^{-1} southward winds and generated waves over 5 m high. Alongshore current speeds, which typically averaged 2–3 cm s^{-1}, surged above 20–30 cm s^{-1}, as wind and current action maintained 10–30 mg L^{-1} TSM shoreline turbidity plumes (Rao et al. 2002). The initial nearshore plume appeared on 09 March 1998. Resuspension increased again on 18 March during

a sustained southward wind of 10 m s^{-1} and persisted for almost 2 months, disappearing in late April. The well-developed coastal plume extended over 300 km from Milwaukee, Wisconsin to Muskegon, Michigan (Fig. 3). During the March event, the estimated total resuspended sediment mass was 7.53×10^9 kg (sediment trap data; Eadie et al. 2002). Under prevailing north to northwest winds, sediments resuspended from wave action would rotate counterclockwise around the southern basin in the nearshore plume. Under moderate wind conditions, coastline irregularities would cause sediments to move offshore near St. Joseph.

When winter storms were very intense, as in 1998, the third episodic phase could be distinguished (Fig. 3). The two rotating gyres set up a convergence zone along the downwind shore that drew resuspended sediments offshore. The large 10 March 1998 storm created greater wave action and stronger counterclockwise alongshore currents. The combination of wave action and currents encouraged plume development well past St. Joseph up to Muskegon, where the coastal plume was captured in the convergence zone of the two-gyre system and drawn offshore. Plume advection into the southern gyre created a spectacular swirling eddy on 12–20 March 1998. Deployed arrays (acoustic Doppler current profilers, smart acoustic current meters, vector-averaging current meters, Argonne National Laboratory tripod) along the eastern coastline documented that during these incursions the alongshore currents increased from a mean of 2–3 cm s^{-1} to over 20 cm s^{-1}, whereas cross-shore currents increased to 4 cm s^{-1} (Murthy et al. 2002). At South Haven, where TSM was over 10 mg L^{-1}, current speed was over 30 cm s^{-1} and wave-current shear stress exceeded 6 dynes cm^{-2}. Above 20 cm s^{-1}, bottom sediments would start to resuspend (Lesht and Hawley 2001).

Enhanced TSM tracks along the gyre correlated spatially with elevated Chl *a* concentrations. Correlated tracks (Figs. 2, 3) strengthen the association between entrained coastal waters, resuspended sediments, and Chl *a* enhancement. However, our analysis of images over several years showed that the doughnut feature was found every year, not just in years with large winter storms. Hence, we surmise that gyre circulation routinely entrains coastal river water discharges, yet only resuspends and entrains coastal plume material during severe storm intervals.

A satellite image from the visible band (TSM) of the MODIS instrument on 23 April 2003 (Fig. 4) illustrates the situation where a doughnut structure is apparent in the central part of the southern basin and a new area of turbid water has been created in the nearshore region. The doughnut structure contains material that was resuspended several weeks earlier from a storm on 04–05 April. Relatively clear water is moving southward along the western coastline off Waukegan to Chicago and northward along the eastern coastline off Michigan City to South Haven, toward the convergence zone. The nearshore turbidity plume is characterized by tendrils of turbid nearshore water that extend offshore in the southeastern part of the basin off St. Joseph. Southward currents along the western nearshore zone carry newly resuspended bottom material into the St. Joseph region. Eventually, this material reinforced the ring structure in the central part of the basin. Although this image is only one example of the recurrent ring-shaped pattern of turbidity seen annually in Lake Michigan, the image clearly distinguishes the offshore doughnut structure from the nearshore coastal sediment plume while underscoring the spatial heterogeneity present in the winter system.

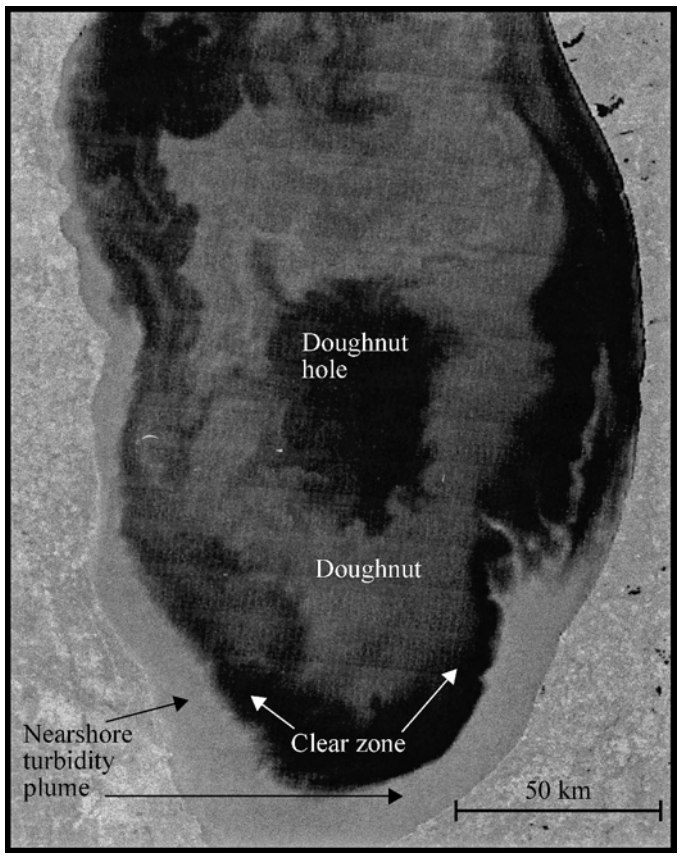

Fig. 4. MODIS image of late-winter doughnut structure in southern Lake Michigan. Image is enhanced to highlight details of offshore TSM ring structure relative to nearshore coastal plumes studied previously by NOAA/NSF EEGLE project. Note the clear central and bordering regions, as well as vorticity eddies off rotating interior columns of the gyre.

Transect reveals vertical structure—The late winter Seabird CTD casts traversed across the southern basin on a longitudinal transect (Fig. 1), sampling 64 stations at 1.85-km (1 nautical mile) intervals, between 86.320°W and 87.745°W (i.e., off St. Joseph, Michigan, to a point off Waukegan, Illinois). On 19–21 April the doughnut was well formed and the cruise path cut across the hole of the structure (Fig. 2a,b), whereas on 12–15 April 2006, it intersected the southern ring.

Both transects (1) confirmed the complex surface spatial pattern of the doughnut and (2) revealed an underlying vertical structure (Fig. 5). At the time of both transects, a thermal bar was beginning to form along the eastern and western coastal margins of southern Lake Michigan, as nearshore temperatures exceeded 4°C, typical for this time

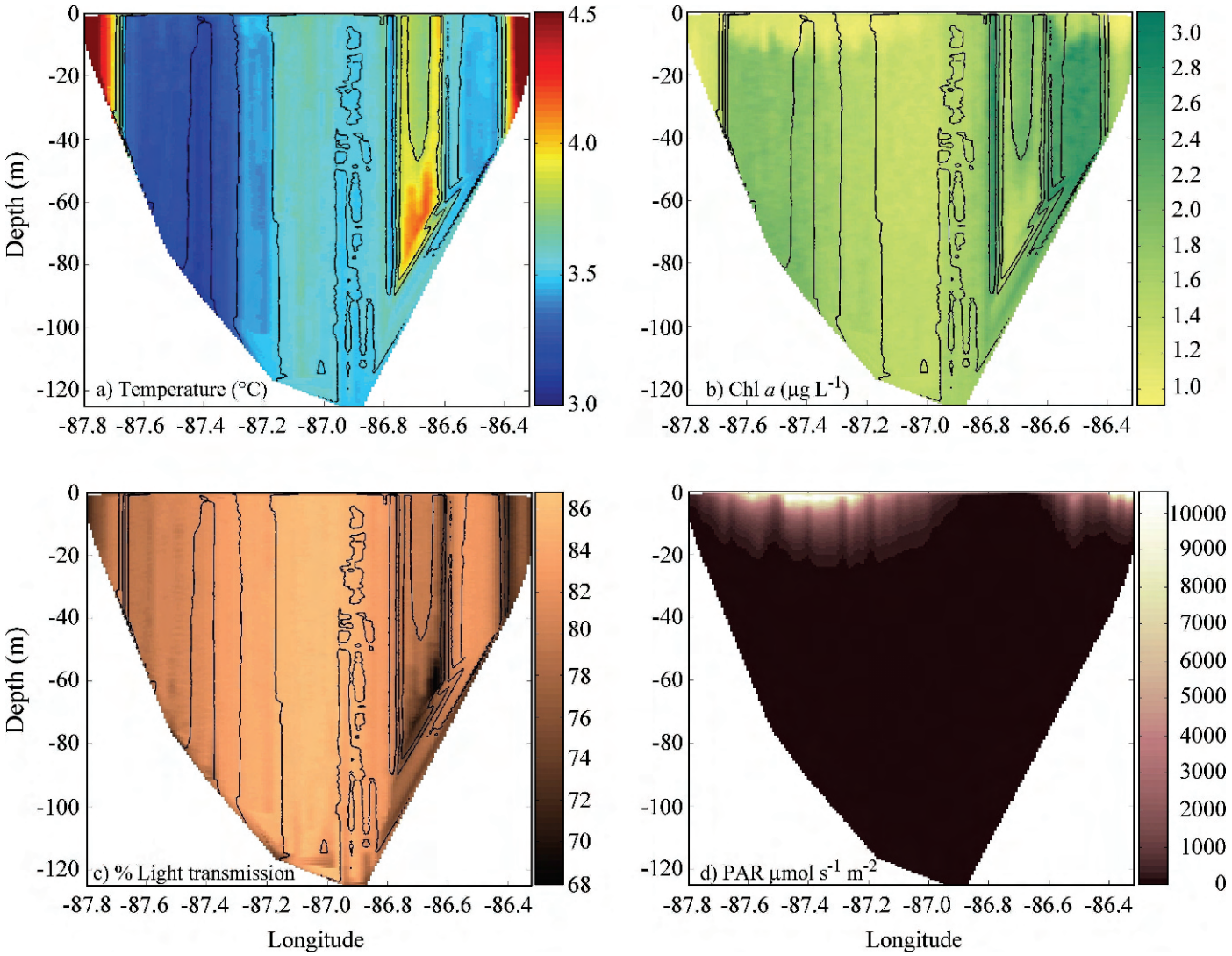

Fig. 5. Vertical structure of the doughnut as revealed by 64 1.85-km (1 nautical mile) Seabird CTD casts along an east–west transect on 19–20 April 2001 (Figs. 1–2, off South Haven, Michigan, to Waukegan, Wisconsin). Panels show (a) temperature, (b) Chl *a*, (c) transmissivity (X-miss), and (d) PAR. Temperature isoclines are superimposed upon Chl *a* and transmissivity plots. Note the vertical structure of Chl *a*, temperature, and transmissivity. Note also that diurnal changes in day/night illumination (PAR) correspond to shallow chlorophyll bleaching along the ship transect.

of year (Chen et al. 2002; Ji et al. 2002). Yet the nearshore coastal regions were not characterized by greatly elevated Chl *a* concentrations, as plankton blooms were just beginning to develop behind the thermal bar and the water was still very turbid (60–70% transmissivity). Rather, we found elevated Chl *a* regions offshore. Along the traverse, the doughnut regions were vertically oriented columns, consistent with complex gyre rotation (Fig. 5a–c). Subtle temperature changes of 0.2°C in the water column were associated with Chl *a*-enriched and Chl *a*-reduced regions in a complex vertical fashion. In the 19–21 April 2001 vertical Seabird CTD transect, the central region (doughnut hole) was 3.4–3.7°C, with low Chl *a* (fluorescence 0.06–0.08; 0.09–1.4 μg Chl *a* L^{-1}) and high transmissivity (>85%). The surrounding doughnut region was composed of slightly cooler water (3.2–3.6°C) with distinct columns of relatively high Chl *a* (fluorescence 0.09–0.14; Chl *a* 1.6–2.6 μg L^{-1}). The subtle depth-related temperature and Chl *a* gradients within this region (1) appeared to distinguish separate water masses, with (2) vertical phytoplankton mixing (i.e., below the PAR zone) within the columns (note temperature overlay; Fig. 5a–c). Between the doughnut and the coastal thermal bar region, there was a thin lens of less productive water (fluorescence 0.05–0.07; Chl *a* 0.7–1.1 μg L^{-1}).

The CTD profiles also suggested photo-quenching during daylight hours, coinciding with high incident radiation (PAR) in surface waters (0–10 m depth; 09:00–16:00 h eastern standard time). The high PAR profiles (Fig. 5d) matched reductions of fluorescence response per unit chlorophyll in shallow depths (Fig. 5b) as the ship passed from day to night (Fig. 5d). Clear versus cloudy conditions also contributed to diurnal variability.

Concern that interpolation between vertical CTD casts might tend to exaggerate the vertical nature of the

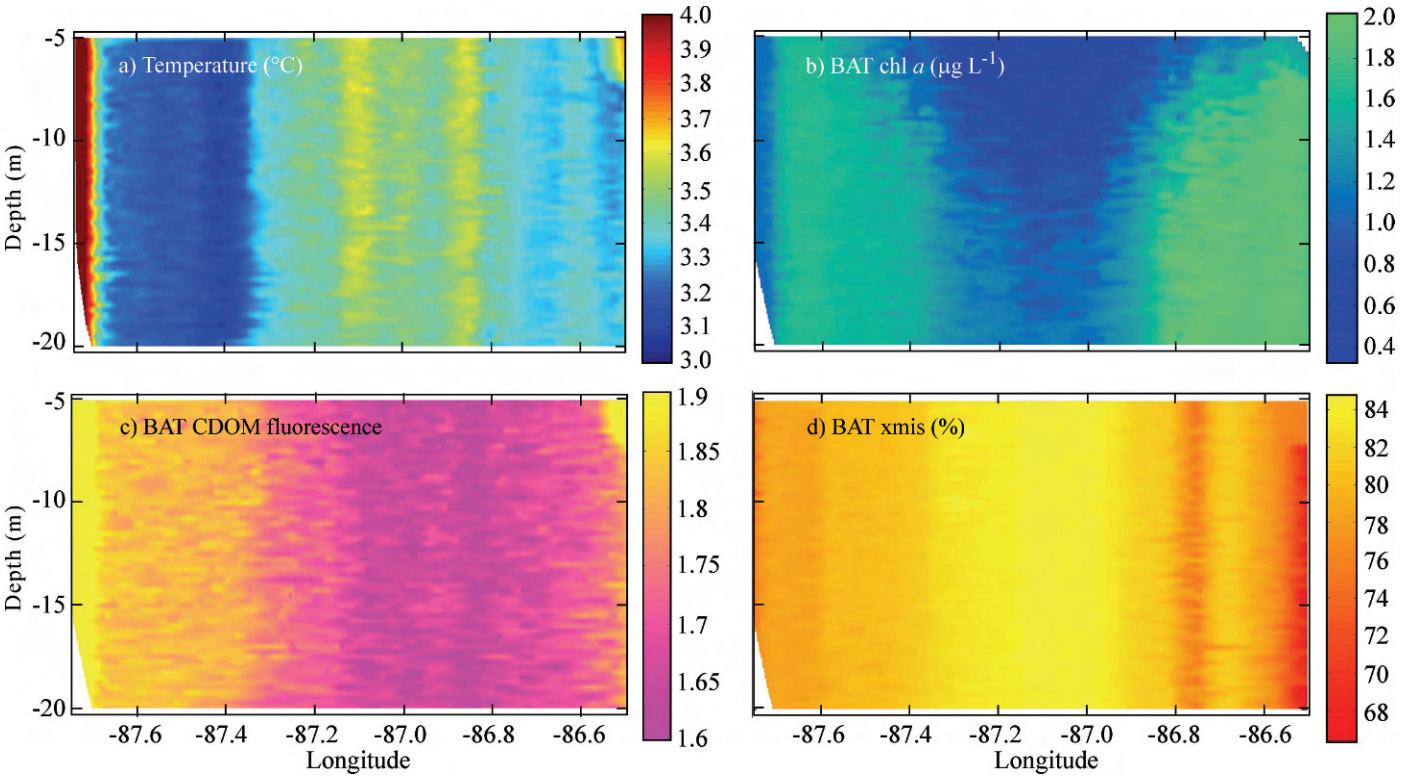

Fig. 6. Return BAT tow-yo transect west to east through the doughnut, over 5–20-m depth. Panels show (a) temperature, (b) Chl *a*, (c) dissolved organic matter (DOM) fluorescence, and (d) transmissivity (X-miss). Note that the BAT variables also show a strong columnar (gyre) structure along the ship transect.

doughnut structure prompted us to execute horizontal transects. The horizontal BAT tows became important as a simultaneous, independent test of vertical structure. Although limited in vertical extent to 5–20-m depth, the BAT tows clearly verified a strong vertical orientation to the doughnut pattern, providing independent evidence for gyre effects (Fig. 6). Vertical orientation was present in all sensitive variables: Chl *a*, temperature, CDOM fluorescence, and transmissivity. The doughnut was distinguished by elevated Chl *a* concentrations (1.2–2.2 μg L^{-1}) from surface to depth, again with clearer waters (Chl *a* 0.4–0.8 μg L^{-1}) in the central hole region. Again there were subtle (0.2°C) yet vertical temperature differences between regions. Whereas the western thermal bar ranged from 3.9°C to >4.0°C, intervening waters were 3.0–3.2°C, doughnut waters were 3.0–3.4°C, and hole waters were 3.6–3.7°C. Nearshore coastal regions showed relatively high temperatures (thermal bar) and high CDOM, characteristic of riverine inputs (Fig. 6c; also see Cotner et al. 2000; Bergmann et al. 2004). The CDOM pulse along the western margin of the doughnut (Fig. 6c) possibly marked a column of captured river water.

On-site and laboratory calibration studies during the 12–15 April 2006 cruise again verified elevated Chl *a* in the doughnut structure, suggesting values ranging between 1.0 and 2.4 μg L^{-1} (Table 2; Fig. 7). On these dates, the transect passed through the southern ring of the doughnut, again showing marked spatial heterogeneity in Chl *a* and other variables marked by subtle changes in temperature. Once again the vertical CTD casts and horizontal BAT tows suggested that the doughnut structure was composed of vertical columns of clear water and phytoplankton-enriched regions related to the winter gyre structure. As before, the regions extended from near the surface to bottom layers. Statistical plots (standard deviations) of temperature, Chl *a*, and light transmission values for the CTD vertical casts demonstrate the heterogeneous vertical structure for variables across the cruise transect (Fig. 7).

The vertical patterns are consistent with the view that entrained PO_4-enriched coastal waters, resuspended sediment, and bacteria are drawn laterally and vertically into the southern gyre by circulation, promoting late-winter phytoplankton growth. Moreover, the CTD casts suggest that the gyre rotation (vorticity) created vertically mixed columns that distributed phytoplankton down to the deepest water regions, far below PAR penetration.

Phytoplankton from our net tows and water samples documented that the species composition in the doughnut had spring bloom components (abundant large diatoms: *Melosira* [*Aulacosira*], *Asterionella, Tabellaria, Fragilaria*), in addition to the typical open-water small centric diatoms (*Cyclotella*), cryptophytes, and flagellates (Millie et al. 2003; Bergmann et al. 2004). The persistent autotrophic vertical structure creates interesting implications for late-winter food-web interactions (zooplankton, fish).

Zooplankton patterns—Was the late-winter ring of Chl *a* associated with variations of organisms higher in the food

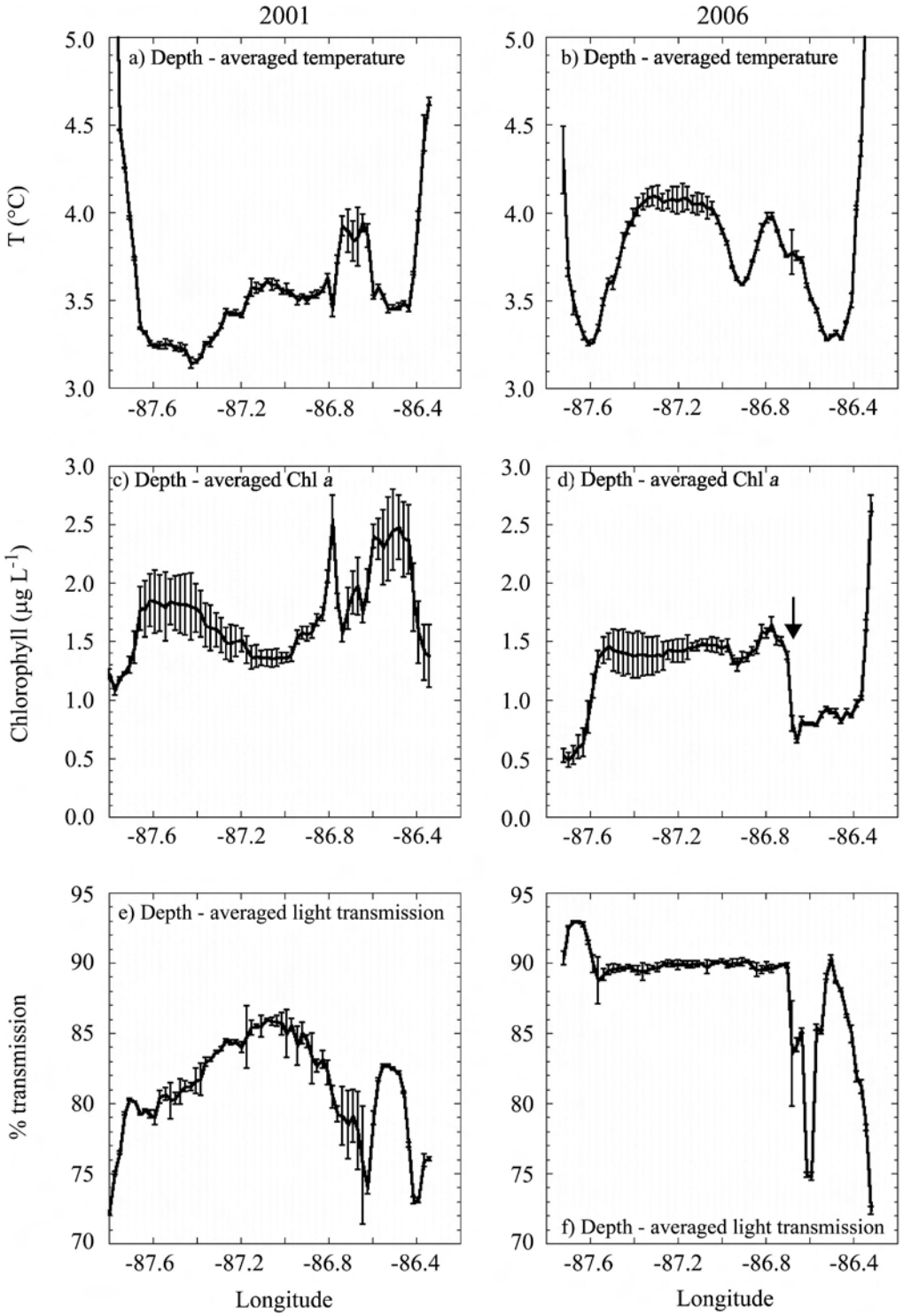

Fig. 7. Statistical plots for (a, b) temperature, (c, d) Chl *a*, and (e, f) transmissivity CTD vertical casts (19–21 April 2001 and 12–15 April 2006 mid-lake cruises). Seabird CTD values are means and standard deviations for vertical series displayed along the longitude transect. In 2001, the transect cut across the doughnut hole (Fig. 2a), whereas in 2006 it cut across the southern ring. Chl *a* scale is derived from Seabird CTD fluorescence, calibrated against shipboard Chl *a* determinations (Table 2). Arrow indicates high abundance of fish (sonar).

chain? Initial evidence for this first came from the 19–21 April 2001 OPC tallies on the BAT tows. The OPC registered intriguing horizontal differences in zooplankton size distributions along the cruise transect. Across the transect, concentrations averaged 10,684 (SD = 1,119) total organisms m^{-3}, with a mean of 6,845 (SD = 1,169) counts m^{-3} for bin 1 and 3,831 (SD = 914) counts m^{-3} for bin 2. When the separate counts from bins 1 (small, 0.250–

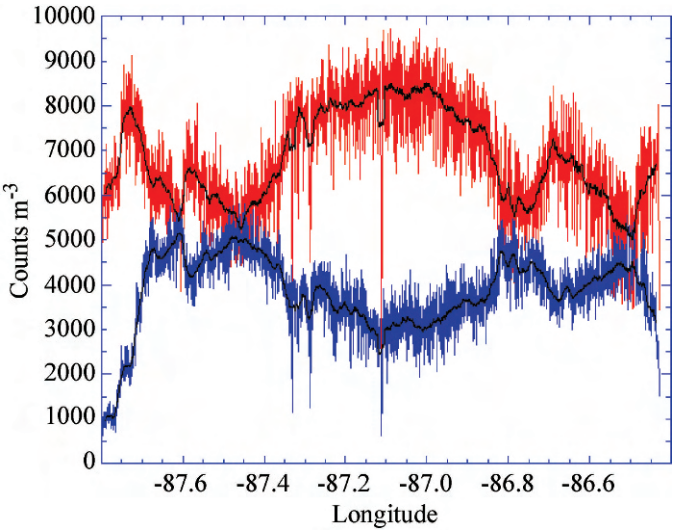

Fig. 8. OPC results from 19–20 April 2001 transect across southern Lake Michigan. Note the inverse patterns in small-size (0.250–0.500 mm ESD, red) and large-size (0.500–1.000 mm ESD, blue) zooplankton counts. Data from 10-s recording intervals are plotted on a 50-interval running mean with high–low ranges. Although autocorrelation is a concern, individual bin 1 tallies for west doughnut versus hole gave mean ± 1 SE counts of 5,945 ± 21 (n = 862), compared with 8,038 ± 20 (n = 2,195; ANOVA F_1 = 4,902, $p < 0.0001$) and the same for east doughnut versus hole (n = 1,717; F_1 = 2,525; $p < 0.0001$). On the other hand, bin 1 comparisons between west and east doughnut limbs were not significantly different (west 5,945 ± 21, east 5,958 ± 34; n = 1,245, F = 0.12, p = 0.73).

0.500 mm) and 2 (large, 0.500–1.000 mm;) were compared, smaller-bodied zooplankters (e.g., rotifers, copepod nauplii) were more abundant in the hole region, whereas larger-bodied zooplankters (e.g., diaptomid copepodites) were more abundant in the doughnut (Fig. 8). Figure 8 shows ranges and a running mean (50-interval) across the cruise transect, expressed as organisms m^{-3}. Although spatial autocorrelation is a concern with OPC data sets, analysis of variance (ANOVA) tests run on 10-s interval counts from various zones (doughnut vs. central hole, peripheral "clear zone") showed highly significant differences. Because bin 2 organisms were larger in volume, total zooplankton biomass appeared greater in the doughnut region, although there were indications of an inverse relationship between larger and smaller organisms (perhaps predation by cyclopoids, *Epischura*, and *Limnocalanus* on immature stages). Thus, there was strong evidence for spatial heterogeneity at the zooplankton trophic level and several patterns coincided with the doughnut structure.

As mentioned earlier, vertical plankton tows with 75-μm or 125-μm zooplankton nets in the doughnut region were often fouled with large diatoms (*Melosira* [*Aulacosira*], *Asterionella*, *Tabellaria*, *Fragilaria*) typically associated with nearshore spring blooms. On the 12–15 April 2006 cruise, 125-μm vertical tows indicated a marked increase in zooplankton abundance that coincided with the doughnut ring (Table 4). Comparison of net tows within the doughnut ring with tows from surrounding clear waters

Table 4. Densities (number m^{-3}) of plankton in southern doughnut ring and outside (eastern, western sides), in surrounding clear-water region (13–14 April 2006 S. Lake Michigan sampling transect). The 2006 transect missed the doughnut hole, and cut across the southern ring. Clear, cold-water samples came from both eastern and western clear-water zones outside of the doughnut ring. Densities are means ±95% confidence limits (n = 9 in doughnut ring, n = 15 outside; see text for discussion of biological categories).

Taxa	Inside ring	Outside ring
Nauplii	8,894±1,754	1,867±498
Diaptomus	5,017±999	1,127±422
Cyclopoids	217±74	160±54
Omnivores	422±280	127±63
Dreissena	900±472	60±30

revealed horizontal differences related to abundance of nauplii, diaptomid copepodites (*Leptodiaptomus sicilis, Leptodiaptomus siciloides*), and adult omnivorous copepods (*Epischura lacustris, Eurytemora affinis, Limnocalanus macrurus*). On this transect, nauplii (4.7× more enriched; ANOVA $F_{9,15}$ = 115.4; $p = 3.2 \times 10^{-10}$) and diaptomid copepods (4.4×; ANOVA $F_{9,15}$ = 86.6; $p = 4 \times 10^{-10}$) were significantly more abundant in the doughnut ring, as were omnivorous adult copepods (2×; ANOVA $F_{9,15}$ = 8.7; p = 0.007). Enrichment of *Leptodiaptomus sicilis* in the rings is interesting, as this species is capable of ingesting large diatoms (*Melosira* [*Aulacosira*], *Asterionella*). Cyclopoid copepods were not significantly enriched (ANOVA $F_{9,15}$ = 1.9; p = 0.18). Moreover, plankton samples along the cruise transect contained pelagic mussel larvae (Quagga mussels, *Dreissena bugensis*). *Dreissena* larvae were significantly enriched in the doughnut ring (ANOVA $F_{9,15}$ = 28.5; $p = 2.31 \times 10^{-10}$), achieving densities nine times higher than in surrounding clear water (Table 4). A final spatial heterogeneity found in the 2006 cruise was a marked increase in sonar targets (fish) at the edge of the doughnut ring (arrow in Fig. 7).

Phosphorus sources—Where are the nutrients coming from that stimulate the doughnut ring? Relative to offshore water and sediments, river discharges were high in TDP and coastal sediments were enriched in TP (Table 3; also Cotner et al. 2000; Biddanda and Cotner 2002). In incubation experiments simulating sediment resuspension and river-water entrainment, statistically significant enhancement of primary productivity (i.e., ΔPOC, with bacterial production removed) occurred in all the experimental treatments (+Sediment, +River, and +River+Sediment) relative to the lake water control (Fig. 9). The enhancement of PP was most pronounced in the +River+Sediment treatment (~10-fold), followed by the +River (~8-fold) and the +Sediment (~3-fold) treatments.

Discussion

Thus spatial structure in southern Lake Michigan during late winter to early spring indicates strong connections between physical and biological dynamics. Rather than

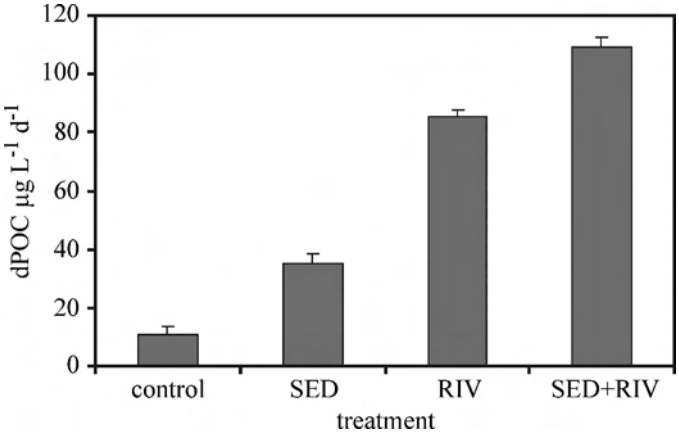

Fig. 9. Primary production in incubation (microcosm) experiments, measured as ΔPOC μg L^{-1} d^{-1} minus bacterial production. Primary production is stimulated by river water (RIV) and by resuspended dilute coastal sediments (SED), but most by a combination of both river water and coastal sediments (SED+RIV). Standard error bars are shown for mean concentrations (*t*-test; $n = 3$; SED $t = 9.2$, $p = 3.31E\text{-}06$, RIV $t = 12.7$, $p = 1.71E\text{-}08$, SED+RIV $t = 41.4$, $p = 1.6E\text{-}122$).

uniformly mixed, homogeneous waters, wind-driven gyre circulation sets up a rotating vertical structure that is characterized by alternating turbid (TSM, Chl *a*) and clear water columns. The turbid strata evident in remote sensing images extend to bottom sediments and are correlated with subtle differences in temperature, indicative of rotating water columns. A ring of phytoplankton production (the doughnut) forms in late winter, associated with coastal entrainment episodes.

The doughnut production pulses can be distinguished from studies of ''spring blooms'' in southern Lake Michigan by timing and location. The traditional spring bloom is associated with river waters captured behind the developing spring thermal bar and is an ecologically important event, contributing up to 50% of the total annual PP of the lake and a major source of carbon to higher trophic levels. Light and phosphorus availability appears to control phytoplankton growth and abundance in typical spring blooms behind the thermal bar (Fahnenstiehl and Scavia 1987). Recent detailed studies of light attenuation, sediment, and nutrient concentrations suggest that light limitation from nearshore coastal sediment plumes constrains phytoplankton growth during large nearshore plume years (Lohrenz et al. 2004). However, sediment resuspension supports enhanced heterotrophic bacterial production in the coastal region (Cotner et al. 2000; Biddanda and Cotner 2002) and DOC tributary inflows contribute to production behind the thermal bar (Cotner et al. 2000; Lohrenz et al. 2004).

At this time, the doughnut phenomenon poses more questions than it provides answers. How much river discharge and coastal sediments are captured and transferred offshore? How long has the process been going on? Is there deep scour of the coastal shelf associated with rotating gyre (vorticity) effects? Crucial to any deep scour argument is more information about shear stresses and sediment resuspension, since remote sensing studies record only what is happening in surface waters (Beletsky et al. 2003). Models and data from 18 moorings deployed between 1998 and 2000 suggest that wave-driven resuspension can reach down to 50–80-m depth, and that storm-driven currents can resuspend sediments, but that the stress required for resuspension is very dependent upon the properties of the sediment (Lesht and Hawley 2001).

One important consequence of the doughnut concerns winter productivity. Although the spatial patterns of the doughnut involve differences of only 2 μg L^{-1} Chl *a*, the greater vertical extent of deep-water regions relative to shallow-water regions suggests that total phytoplankton biomass might actually be greater in the offshore rings than in the traditional spring bloom behind the thermal bar (Budd et al. pers. comm.). Moreover, any preliminary calculations of phytoplankton biomass are likely low-biased because of ocean algorithms underestimating central Lake Michigan Chl *a* concentrations by 40–50%, related to an underestimate of cryptophyte pigments (phycobilin) that vary from traditional blue : green reflectance ratios (Bergmann et al. 2004). Because winter offshore waters are much deeper than the photic zone and much colder than nearshore spring-bloom waters, productivity of algae will probably be much less per biomass. However, Cotner and colleagues (Cotner et al. 2000; Biddanda and Cotner 2002) found that DOC-stimulated bacterial production from nearshore plume water was 64% of rates measured in August, so that early on (January–March), heterotrophic activity may be fueling PO_4 transfers.

Although limited in extent, our late-winter mesocosm experiments simulated river-water entrainment and coastal sediment resuspension. The results demonstrated the potential for such processes to influence autotrophic primary production. The higher stimulation of PP by river water compared with resuspended coastal sediment probably reflects the higher availability of PO_4. Whereas primary productivity was stimulated by both river water and resuspended sediment, it was stimulated most (~10-fold over ambient lake-water rates) by a combination of coastal sediments and riverine water, the natural mix found along gyre convergence zones. Earlier, we observed that Chl *a* increases occur along spatial tracks that correspond to entrained dilute TSM concentrations (Figs. 2, 3). As in the incubation experiments, the entrained particles probably continue to be converted to inorganic nutrients via remineralization or the nutrient-rich bacteria are directly ingested by cryptophytes, which normally dominate in deep-water, central regions, and nutrients are subsequently released during food-web interactions (Cotner et al. 2000; Millie et al. 2003; Bergmann et al. 2004). The mesocosm experiments reinforce the notion that episodic coastal entrainment could have a lakewide effect as materials are transported rapidly offshore by recurring storm events.

The river-water/coastal sediment incubation results are similar to previous findings from Lohrenz et al. (2004), who also conducted enrichment experiments with St. Joseph River water and coastal sediments. Chlorophyll and carbon-specific growth rates were highest in treatments with river water augmented with sediments, high with river

water alone, and slight but significant with sediment alone. However, the studies of Lohrenz et al. were directed toward nearshore turbidity plumes. They suggested that the high turbidity found in nearshore plumes could act to suppress early spring algal productivity behind the developing thermal bar. In contrast, we argue that the lower turbidity values in the convergence zone and offshore gyre ring act to stimulate offshore productivity. That is, when major offshore excursions of sediment (TSM) are entrained in the gyre, only river water and small particles in dilute concentrations are transported over great distances. Entrainment of nutrient-rich coastal waters and the decomposition of resuspended fine benthic particles (bacteria and detritus) are probably responsible for Chl *a* responses in the doughnut (Biddanda and Cotner 2002; Ji et al. 2002; Chen et al. 2004).

Some of the biological implications are intriguing. The bacteria, cryptophytes, and small centric and large pennate diatoms of the doughnut are probably consumed by copepods and heterotrophic protozoans (Cotner et al. 2000; Biddanda and Cotner 2002; Vanderploeg et al. 2007). Timing here could be crucial for life cycles of species. At the very season when resources are most scarce (e.g., late winter, unstratified period), offshore productivity may alleviate starvation of overwintering zooplankton. Several of the larger-bodied calanoid copepod species overwinter (*Leptodiaptomus sicilis, Limnocalanus macrurus, Eurytemora affinis, Senecella calanoides*) and are characteristic of the Laurentian Great Lakes. These larger-bodied species include winter life stages that draw from lipid or wax ester reserves for both survival and for clutch size in early spring (Vanderploeg et al. 1992). Some of the larger species (e.g., *Limnocalanus macrurus*) are omnivorous. Whereas previous explanations of alternative life history success have centered on temperature and hypolimnetic algal production in addition to taste discrimination of suspended particles (Vanderploeg et al. 1992; Kerfoot and Kirk 1993), the discovery of the late-winter doughnut provides a potentially new insight, one that separates the Great Lakes from winter resource patterns in smaller lakes. That is, adult females in the critical time before releasing broods could be benefiting from enhanced algal productivity rather than passing through a resource bottleneck. By energizing the base of food webs, the late-winter doughnut bloom could reduce competition among grazers, and help maintain overwintering life history stages and, in the long run, promote overall community diversity. In smaller, ice-covered lakes, this option is not available, as snow and ice cover dramatically reduce illumination and wind effects.

Moreover, concentration of zooplankton in the bloom regions could attract larger omnivorous or predatory invertebrates (*Limnocalanus*, mysids) and fish, amplifying the food-web repercussions. In the 2006 transects, recall that there was evidence for enhanced abundance of omnivorous copepods and greatly elevated sonar signals (fish) when the ship passed from the outside clear-water margin into the outside eastern ring of the doughnut.

Long-term trends in the doughnut phenomenon are not known at present, but are under investigation. Global climate studies suggest that greenhouse warming may lead to increased frequency of El Niño events (Timmermann et al. 1999) and associated alterations in weather, including increased frequency and severity of storm events and reduced shoreline ice cover (Hanley et al. 2003). The last 30 yr provide evidence for correlations between coastal ice reduction, increased coastal turbidity, and higher storm frequency (Schwab et al. 2006; Austin and Colman 2007). Although there is great uncertainty in extrapolations, the 1998 observations, which coincided with an El Niño event, emphasize the possibility that climate-mediated weather events could progressively accentuate offshore, late-winter productivity by capturing greater volumes of PO_4-rich river discharges and resuspending greater amounts of PO_4-rich coastal sediments. Loss of coastal ice and diversion of PO_4, POC, and DOC from the coastal margin to deep water may contribute to observed reductions in coastal amphipods (*Diporeia*), since coastal ice protects margins from winter wave action and normally traps high amounts of river POC, DOC, and PO_4 inputs. The doughnut phenomenon might also contribute to a change in offshore stoichiometry. Greater PO_4 input from coastal environments could shift the offshore phytoplankton community composition away from typical small centric diatom and cryptophyte deep-water assemblages toward increased frequency of larger diatom species. In the past, smaller, offshore cryptophyte and centric diatom assemblages were characteristic of the deep offshore waters, although large diatoms have always been present (Lohrenz et al. 2004).

Is the doughnut phenomenon a consequence of recent warming events, reducing shelf ice and progressively diverting nutrients to an offshore gyre system, or has the doughnut existed for a long time and has just gone unnoticed? An urgent regional consideration involves colonization of the littoral region by dreissenid mussels and potential effects on spring bloom productivity as more algae are removed from the nearshore water column. Rather than buffering productivity, the discovery of high concentrations of dreissenid larvae in the doughnut raises the possibility that the offshore phenomenon may contribute to mussel success by elevating mussel survivorship and promoting dispersal of immature life history stages (especially the "profunda" variety of quagga mussels, which settle on deep, soft substrates). The immature stages may disperse as the ring structure collapses in late April.

In any case, discovery of this phenomenon (deep displacement hypothesis) should stimulate research into coupled physical–biological dynamics in many ice-free large temperate lakes, as the dogma of a uniformly mixed water body in winter is tested in many of the Great Lakes. The physics of mixing of different water masses, scouring of benthic sediments, and biotic interactions within entrained plumes all require greater scrutiny and three-dimensional study. There is evidence from winter ice surveys of reduction in coastal ice during the last four decades (Assel 2003). There is also evidence from SeaWiFS imagery for coastal entrainment effects in other Great Lakes, although shoreline geometry modifies site-specific circulation patterns. For example, SeaWiFS imagery from 24 March 1998 shows offshore movement of sediments and algae in southern Lake Huron (out of Saginaw Bay, up from Port

Huron), Lake Erie (transfer from the shallow western basin into the deeper eastern basin), along the southern shore of Lake Ontario, and in Lake Superior (out of Duluth, through the Apostle Islands and off the western coast of the Keweenaw Peninsula). Whereas we have considered Chl *a* and TSM from remote sensing imagery, the question of PO_4 sources, the timing of transition from heterotrophic to autotrophic productivity, and the favoring of different types of bloom communities are also major questions. We suspect that winter transfer of littoral PO_4, DOC, and POC into deeper waters is accelerating in all the Great Lakes, but is more pronounced in the southern lakes. Resulting late-winter pulses could create perturbations that travel from the base of the food web to the very top, encompassing a whole host of interesting late-winter interactions that play out in space and time.

References

Assel, R. A. 2003. Recent trends in Laurentian Great Lakes ice cover. Clim. Change **57:** 185–204.

Austin, J. A., and S. M. Colman. 2007. Lake Superior summer water temperatures are increasing more rapidly than regional air temperatures: A positive ice–albedo feedback. Geophys. Res. Lett. **34:** L06604, doi:10.1029/2006GL029021.

Beletsky, D., and D. J. Schwab. 2001. Modeling circulation and thermal structure in Lake Michigan: Annual cycle and interannual variability. J. Geophys. Res. **106:** 19745–19771.

———, D. J. Schwab, P. J. Roebber, M. J. McCormick, G. S. Miller, and J. H. Saylor. 2003. Modeling wind-driven circulation during the March 1998 sediment resuspension event in Lake Michigan. J. Geophys. Res. **108:** 3038, doi:10.1029/2001JC001159.

Bergmann, T., G. Fahnenstiel, S. Lohrenz, D. Millie, and O. Schofield. 2004. Impacts of a recurrent resuspension event and variable phytoplankton community composition on remote sensing reflectance. J. Geophys. Res. **109:** C10515, doi:10.1029/2002JC001575.

Biddanda, B. A., and J. B. Cotner. 2002. Love handles in aquatic ecosystems: The role of dissolved organic carbon drawdown, resuspended sediments, and terrigenous inputs in the carbon balance of Lake Michigan. Ecosystems **5:** 431–445.

Budd, J. W., W. C. Kerfoot, S. Green, and M. Julius. 2002. News. Ocean Color Spectrum, Spring/Summer, 33–34.

———, and D. S. Warrington. 2004. Satellite-based sediment and chlorophyll a estimates for Lake Superior. J. Great Lakes Res. (suppl. 1) **30**: 459–466.

———, D. S. Warrington, V. Ransibrahmanakul, and J. D. Chye. 1999. Episodic events and trophic pulses: Estimating surface chlorophyll concentrations and transport using SeaWiFS imagery. Eos Trans. AGU, 80(49), Ocean Sci. Meet. Suppl., OS41C-13.

Chen, C., and others. 2002. A model study of the coupled biological and physical dynamics in Lake Michigan. Ecol. Model. **152:** 145–168.

———, and others. 2004*a*. Impacts of suspended sediment on the ecosystem in Lake Michigan: A comparison between the 1998 and 1999 plume events. J. Geophysical Res. **109:** C10S05, doi:10.1029/2002JC001687.

Cotner, J. B., T. H. Johengen, and B. A. Biddanda. 2000. Intense winter heterotrophic production stimulated by benthic resuspension. Limnol. Oceanogr. **45:** 1672–1676.

Davis, C. O., and M. S. Simmons. 1979. Water chemistry and phytoplankton field and laboratory procedures. Spec. Rep. 70, Great Lakes Res. Div., Univ. of Michigan.

Eadie, B. J., and others. 1996. Anatomy of a recurrent episodic event: A winter-spring plume in southern Lake Michigan. EOS. Transactions of the American Geophysical Union **77:** 337–338.

———, and others. 2002. Particle transport, nutrient cycling, and algal community structure associated with a major winter-spring sediment resuspension event in southern Lake Michigan. J. Great Lakes Res. **23:** 324–337.

Fahnenstiehl, G., and D. Scavia. 1987. Dynamics of Lake Michigan phytoplankton: Primary production and growth. Can. J. Fish. Aquat. Sci. **44:** 499–508.

Gregg, W. W. 1992. Analysis of orbit selection for SeaWiFS: Ascending vs decending node. NASA Tech. Memo 104566. Vol. 2, 16 pp.

Gumley, L., J. Descloitres, and J. Schmaltz. 2003. Creating reprojected true color MODIS images: A tutorial. Version 1.0. November 14, 2003.

Hagerthey, S. E., and W. C. Kerfoot. 1998. Groundwater flow influences the biomass and nutrient ratios of epibenthic algae in a north temperate seepage lake. Limnol. Oceanogr. **43 (6):** 1227–1242.

Hanley, D. E., M. A. Bourassa, J. J. O'brien, S. R. Smith, and E. R. Spade. 2003. A quantitative evaluation of ENSO indices. J. Clim. **16:** 1249–1258.

Ji, R., and others. 2002. Influences of suspended sediments on the ecosystem in Lake Michigan: A 3-D coupled bio-physical modeling experiment. Ecol. Model. **152:** 169–190.

Kerfoot, W. C., J. W. Budd, B. J. Eadie, H. A. Vanderploeg, and M. Agy. 2004. Winter storms: Sequential sediment traps record *Daphnia* ephippial production, resuspension and sediment interactions. Limnol. Oceanogr. **49:** 1365–1381.

———, and K. L. Kirk. 1993. Why the hypolimnion is not a desert: The taste discrimination-temperature hypothesis. Verh. Internat. Verein. Limnol. **25:** 335–343.

Leshkevich, G. A., D. J. Schwab, and G. C. Muhr. 1993. Satellite environmental monitoring of the Great Lakes: A review of NOAA's Great Lakes Coast Watch Program. Photogrammet. Eng. Rem. Sens. **59:** 371–380.

Lesht, B. M., and N. Hawley. 2001. Using wave statistics to drive a simple sediment model, p. 1366–1375. *In* Proceedings of the Fourth International Symposium Waves 2001, Ocean wave measurement and analysis. Am. Soc. of Civ. Eng.

Lohrenz, S. E., G. L. Fahnenstiel, D. F. Millie, O. M. E. Schofield, T. Johengen, and T. Bergmann. 2004. Spring phytoplankton photosynthesis, growth, and primary production and relationships to a recurrent coastal sediment plume and river inputs in southestern Lake Michigan. J. Geophys. Res. **109:** C10S14, doi:10.1029/2004JC002383.

McClain, C. R., M. L. Cleave, G. C. Feldman, W. W. Gregg, S. B. Hooker, and N. Kuring. 1998. Science quality SeaWiFS data for global biosphere research. Sea Technology Reprint.

Menzil, D. W., and N. Corwin. 1965. The measurement of total phosphorus liberated in seawater based on the liberation of organically bound fractions by persulfate oxidation. Limnol. Oceanogr. **10:** 280–281.

Millie, D., G. L. Fahnenstiel, S. E. Lohrenz, H. J. Carrick, T. Johengen, and O. M. E. Schofield. 2003. Physical–biological coupling in south-eastern Lake Michigan: Influence of episodic sediment resuspension on phytoplankton. Aquat. Ecol. **37:** 393–408.

Mortimer, C. H. 1988. Discoveries and testable hypotheses arising from Coastal Zone Color Scanner imagery of southern Lake Michigan. Limnol. Oceanogr. **33:** 203–226.

MURTHY, C. R., Y. R. RAO, M. J. MCCORMICK, G. S. MILLER, AND J. H. SAYLOR. 2002. Coastal exchange characteristics during unstratified season in southern Lake Michigan. Verh. Int. Ver. Limnol. **28:** 1–4.

O'REILLY, J., AND OTHERS. 1998. Ocean color algorithms for SeaWiFS. J. Geophys. Res. **103:** 24937–24953.

———, AND OTHERS. 2000*a*. SeaWiFS postlaunch technical report series, Volume 11, SeaWiFS postlaunch calibration and validation analyses, Part 3, NASA Technical Memorandum.

———, AND OTHERS. 2000*b*. SeaWiFS postlaunch calibration and validation analyses, Part 3. *In* S. B. Hooker and E. R. Firestone [eds.], NASA Technical Memo 2000-206892, Vol. 11, NASA Goddard Space Flight Center.

PASCUAL, M., X. RODO, S. P. ELLNER, R. COLWELL, AND M. J. BOUMA. 2000. Cholera dynamics and El Nino–Southern Oscillation. Science **289:** 1766–1769.

RAO, Y. R., C. R. MURTHY, M. J. MCCORMICK, G. S. MILLER, AND J. H. SAYLOR. 2002. Observations of circulation and coastal exchange characteristics in southern Lake Michigan during 2000 winter season. Geophysical. Res. Lett. **29:** 9–1 to 9–4.

SCHWAB, D. J., D. BELETSKY, AND J. LOU. 2000. The 1998 Coastal Turbidity Plume in Lake Michigan. Estuarine Coast. Shelf Sci. **50:** 49–58.

———, B. J. EADIE, R. A. ASSEL, AND P. J. ROEBBER. 2006. Climatology of large sediment resuspension events in southern Lake Michigan. J. Great Lakes Res. **32:** 50–62.

STUMPF, R. P., R. A. ARNONE, R. W. GOULD, JR, P. M. MARTINOLICH, AND V. RANSIBRAHMANAKUL. 2003. A partially coupled ocean-atmosphere model for retrieval of water-leaving radiance from SeaWiFS in coastal waters. *In* Algorithm updates for the fourth SeaWiFS data reprocessing. Vol. 22, SeaWiFS postlaunch Technical Report Series.

———, V. RANSIBRAHMANAKUL, K. HUGHES, R. SINHA, S. RAMACHANDRAN, AND H. GU. 2000. ESDIM progress report: The evaluation of the atmospheric correction algorithms for processing SeaWiFS data. Project 392N-SeaWiFS Regional Pathfinder: Reproducing validation, and exploitation of SeaWiFS ocean color data.

TIMMERMANN, A., J. OBERHUBER, A. BACHER, M. ESCH, M. LATIF, AND E. ROECKNER. 1999. Increased El Nino frequency in a climate model forced by future greenhouse warming. Nature **398:** 694–697.

VANDERPLOEG, H. A., W. S. GARDNER, C. C. PARRISH, J. R. LIEBIG, AND J. F. CAVALETTO. 1992. Lipids and life-cycle strategy of a hypolimnetic copepod in Lake Michigan. Limnol. Oceanogr. **37:** 413–424.

———, AND OTHERS. 2007. Anatomy of the recurrent coastal sediment plume in Lake Michigan and its impacts on light climate, nutrients, and plankton. J. Geophys. Res. **112:** CO3590, doi:10.1029/2004JC002379.

WARRINGTON, D. S. 2001. Great Lakes chlorophyll and turbidity estimates using SeaWiFS (Sea-viewing Wide Field-Of-View Sensor) imagery. MS thesis, Michigan Technological Univ.

WETZEL, R. G., AND G. E. LIKENS. 2000. Limnological analyses, 3rd ed. Springer.

WILKINSON, L. 2000. SYSTAT: Version 10.0. SPSS.

WU, J., W. SUNDA, E. A. BOYLE, AND D. M. KARL. 2000. Phosphate depletion in the western North Atlantic ocean. Science **289:** 759–762.

Received: 18 December 2006
Accepted: 10 August 2007
Amended: 28 September 2007